

# SEARCHING FOR NEW PHYSICS USING HIGH PRECISION ABSORPTION SPECTROSCOPY; CONTINUUM PLACEMENT UNCERTAINTIES AND $\Delta\alpha/\alpha$ TOWARDS THE QUASAR PHL957

JOHN K. WEBB<sup>†</sup>

Institute of Astronomy, University of Cambridge, Madingley Road, Cambridge, CB3 0HA, UK  
Clare Hall, University of Cambridge, Herschel Rd, Cambridge, CB3 9AL, UK and  
Big Questions Institute, Level 4, 55 Holt St., Surry Hills, Sydney, NSW 2010, Australia

CHUNG-CHI LEE\*

Big Questions Institute, Level 4, 55 Holt St., Surry Hills, Sydney, NSW 2010, Australia

DINKO MILAKOVIĆ

Institute for Fundamental Physics of the Universe, Via Beirut, 2, 34151 Trieste, Italy and  
INAF - Osservatorio Astronomico di Trieste, via Tiepolo 11, 34131, Trieste, Italy

DARREN DOUGAN

Big Questions Institute, Level 4, 55 Holt St., Surry Hills, Sydney, NSW 2010, Australia

VLADIMIR A. DZUBA

School of Physics, University of New South Wales, Sydney, NSW 2052, Australia

VICTOR V. FLAMBAUM

School of Physics, University of New South Wales, Sydney, NSW 2052, Australia

*Submitted XXX; accepted YYY*

## ABSTRACT

Detecting or placing upper limits on spacetime variations of fundamental constants requires quantifying every potential source of uncertainty. We continue our previous study into the impact of continuum variations on measurements of the fine structure constant, here in the context of quasar absorption systems. An automated (hence objective and reproducible) continuum modelling method is reported in an accompanying paper. We apply the method to the  $z_{abs} = 1.7975$  absorption system towards the quasar PHL957. Multiple continuum fits are generated, and for each, we derive independent models of the system, each giving its own measurement of the fine structure constant  $\alpha$ . This process isolates and quantifies the error contribution associated with continuum placement uncertainty. This source of uncertainty, ignored in many previous measurements, arises in two ways: (i) slight local continuum tilt uncertainty generates small line shifts, and (ii) different continuum estimates produce slightly different kinematic structures in the absorption system model. Taking continuum placement uncertainty into account, the new PHL957 measurement we obtain is  $\Delta\alpha/\alpha = -0.53^{+5.45}_{-5.51} \times 10^{-6}$ . This measurement assumes terrestrial magnesium isotopic abundances. Recommendations are provided for future  $\alpha$  measurements. Finally, we also note the potential importance of the effects identified here for future redshift drift experiments.

*Keywords:* Cosmology: cosmological parameters, observations – Methods: data analysis, numerical, statistical – Techniques: spectroscopic – Quasars: absorption lines

## 1. INTRODUCTION

This paper is a companion paper to Lee et al. (2024), in which we introduce an automated continuum fitting algorithm, based on cubic splines, designed for use on high resolution astronomical spectra.

<sup>†</sup>jw978@cam.ac.uk

\*lee.chungchi16@gmail.com

Modelling absorption features in high-resolution quasar spectra requires an estimate of the unabsorbed continuum level. Broadly, there are three options: (1) estimate  $I_{0,\lambda}$  simultaneously with estimating the theoretical  $\tau_\lambda$ , (2) estimate  $\tau_\lambda$  and  $I_{0,\lambda}$  independently, or (3) make a preliminary estimate of  $\tau_\lambda$  and  $I_{0,\lambda}$  and subsequently simultaneously refine the parameters for  $I_{0,\lambda}$  whilst minimising  $\chi^2$  to model  $\tau_\lambda$ . (1) can be applied

but only in limited circumstances: the continuum function must be simple, otherwise it is easy to create degeneracy between  $I_{0,\lambda}$  and  $\tau_\lambda$  unless the absorption feature is flanked by large continuum regions (which may not be the case). (2) can also be used but then the uncertainty estimates for the final absorption line parameters do not reflect continuum uncertainties. (3) alleviates the problems associated with the first two methods and is thus preferred.

For simplicity, consider only rest-frame quantities, i.e. we ignore redshift in this illustrative discussion: let us take the true wavelength of an absorption line to be given by

$$C = \sum_i^n \Delta\lambda_i (I_{0,i} - I_{obs,i}) / \sum_i^n (I_{0,i} - I_{obs,i}), \quad (1)$$

where  $I_{0,i}$  is the true continuum level against which absorption takes place,  $I_{obs,i}$  is the observed intensity,  $\Delta\lambda_i$  is the pixel width of the  $i^{th}$  pixel, and the summations are made over all  $n$  pixels for the absorption line being measured. However, the measured wavelength is

$$C' = \sum_i^n \Delta\lambda_i (I'_{0,i} - I_{obs,i}) / \sum_i^n (I'_{0,i} - I_{obs,i}), \quad (2)$$

where  $I'_{0,i}$  is the fitted continuum. If  $I'_{0,i} \neq I_{0,i}$ , then it may occur that  $C' \neq C$ .

The observed and laboratory wavelengths  $C_\alpha$  and  $C_{lab}$  of an atomic transition are related by

$$\frac{1}{C_\alpha} = \frac{1}{C_{lab}} + q \left( \frac{\alpha^2}{\alpha_{lab}^2} - 1 \right) \quad (3)$$

where  $\alpha$  is the fine structure constant in the measured gas cloud,  $\alpha_{lab}$  is the terrestrial value, and  $q$  is a transition-dependant sensitivity coefficient [Dzuba et al. \(1999\)](#); [Webb et al. \(1999\)](#). Eqs. 1 to 3 illustrate that a continuum placement uncertainty resulting in  $C' \neq C$  causes a measurement in which we would measure  $C'_\alpha \neq C_\alpha$ , emulating a change in the fine structure constant. This effect has been ignored in many previous measurements of the fine structure constant in astronomical targets, yet should not be. We explore this in more detail in [Section 2](#).

In [Section 5](#), the continuum modelling procedure is applied to a quasar spectrum obtained using the Ultra Violet Echelle Spectrograph (UVES) on the Very Large Telescope (VLT). By varying the continuum fitting knot spacings, i.e. generating different continuum models, we explore how variations in the adopted continuum model impact on measurements of the fine structure constant  $\Delta\alpha/\alpha = (\alpha_z - \alpha_0)/\alpha_0$ , where the subscripts  $z, 0$  indicate redshift and the terrestrial value, and where the fine structure constant  $\alpha = e^2/4\pi\epsilon_0\hbar c$  in SI units ([Section 5.2](#)).

The analysis method for quasar absorption systems is necessarily very different to the white dwarf context. White dwarf photospheres produce a large number of narrow, generally weak, often single absorption lines, with known laboratory wavelengths. Whilst the high number density of lines (from multiple species) can result in some lines being blended, the complex kinematic structures seen in quasar absorption systems do not arise

in white dwarf photospheres. In the quasar case, the profile modelling process returns a kinematic structure that depends on the continuum estimate provided. For that reason, it is important to derive independent models for each input continuum estimate when modelling quasar absorption systems.

In [Section 5](#) we present an AI-VPFIT measurement of  $\Delta\alpha/\alpha$  in the  $z_{abs} = 1.7975$  absorption system towards the quasar PHL957. The fully AI method leaves  $\alpha_z$  as a free parameter throughout the model building process, mandatory for an unbiased  $\Delta\alpha/\alpha$  measurement [Webb et al. \(2022\)](#); [Lee et al. \(2023\)](#). This new PHL957  $\Delta\alpha/\alpha$  measurement also, for the first time, includes additional free parameters to allow for a potential wavelength calibration linear distortion [Webb et al. \(2021a\)](#), and checks (using multiple AI-VPFIT fits) for any possible model non-uniqueness effects [Lee et al. \(2021a\)](#).

## 2. CONTINUUM FITTING PROCEDURE

The method we use for obtaining an initial continuum has been presented in detail in [Lee et al. \(2024\)](#). The advantage of (and reason for producing) that method is that it is automated, i.e. there is no interactive involvement beyond initially setting certain internal modelling parameters (or accepting default hard-coded values), and it is thus objective and reproducible. Since a comprehensive description exists elsewhere, only a brief summary is given here.

The method is based on cubic splines. Absorption (or emission) features in the spectrum are identified automatically and their associated pixels removed from the continuum modelling process. The procedure comprises 6 stages. In stage 1, the spectrum is re-binned onto a finer grid and smoothed using convolution with a Gaussian. In stage 2, a preliminary identification of pixels containing absorption (or emission) features is carried out (refined subsequently). The whole process is iterative but neither stage 1 or 2 are involved in further iterations. Since (following stages 1 and 2) the remaining data have gaps (where features were removed), knot positions are redistributed appropriately (in stage 3), to avoid over-fitting in spectral regions where only a few pixels remain. Stage 4 applies Gauss-Newton optimisation to iteratively solve for intensities at each knot position. Stages 5 and 6 involve further parameter refinements, tweaking the parameter updates and number of knots to minimise the objective function ( $\chi^2$ ) optimally, and a final (but detailed) further refinement is carried out, testing for pixels that may have been incorrectly flagged as features, replacing them if so. The algorithm's parameters used in this analysis are as follows: smoothing FWHM  $3\bar{x}$ ,  $\zeta = 3$ ,  $k_{merge} = 1/3$ ,  $n = 10$  (see [Lee et al. \(2024\)](#) for details).

## 3. ASTRONOMICAL AND ATOMIC DATA

For the  $\Delta\alpha/\alpha$  study in this paper, we use the  $z_{abs} = 1.7975$  absorption system towards the well-studied  $z_{em} = 2.7$  quasar PHL957 (or Q0100+1300 or J010311+131617). This quasar has a long and distinguished history, with many papers devoted to it. Milestones include: its discovery (in a stellar survey) [Haro & Luyten \(1962\)](#), M. Schmidt's identification as a quasar, reported in the spectroscopic study by [Lowrance et al. \(1972\)](#), and then a detailed spectroscopic analysis in

Coleman et al. (1976). This absorption system was used for a  $\Delta\alpha/\alpha$  measurement by Webb et al. (2011); King et al. (2012). It was selected for the present study because we had previously found that it yields a small uncertainty and because of the availability of an existing high quality UVES spectrum: the VLT/UVES data for PHL957 used in this study were obtained by Zafar et al. (2013). That paper gives the wavelength coverage, signal to noise, spectral resolution, and other details. The data extraction we use in this paper is from the compilation/re-reductions of Murphy et al. (2019), in which continua are fitted to individual orders during data extraction, normalised and propagated through the co-addition procedure to form a final one-dimensional spectrum. The final one-dimensional spectrum provided in that compilation is thus normalised to unit continuum. We refer to that unit continuum as the “original” continuum. The compilation in Murphy et al. (2019) is large, comprising 467 reduced quasar spectra, and the provision of a basic continuum for each is extremely useful. However, those continua are relatively low order and not generally suitable for detailed studies involving line profile analysis, as we show in the present study.

In the context of the  $\Delta\alpha/\alpha$  measurements made here, the most important atomic data parameters are the laboratory rest wavelengths  $\lambda$  of the absorption transitions used, the oscillator strengths  $f_{ik}$ , damping constants  $\Gamma$ , sensitivity coefficients  $q$ , where the terminology is as given in the VPFIT user guide Carswell & Webb (2023, 2014). The values of all atomic parameters used in the present study are as provided with VPFIT version 12.4 (Carswell & Webb 2023).

#### 4. CONTINUUM MODELS

For the  $z_{abs} = 1.7975$  absorption system towards PHL957 analysed here, the continuum level against which  $\Delta\alpha/\alpha$  is measured is obtained as follows:

- (i) first, prior to absorption line modelling, we derive a new *preliminary* continuum model, then
- (ii) during absorption system modelling, we refine the local continuum estimates (independently for each spectral segment fitted), modifying the preliminary continuum  $I_{0,\lambda}$  using a 2-parameter linear correction, so the final continuum becomes

$$I'_{0,\lambda} = I_{0,\lambda} \left( c_l + c_s \left( \frac{\lambda}{\lambda_{ref}} - 1 \right) \right), \quad (4)$$

where  $c_l$  and  $c_s$  are constants specific to each of the six spectral regions fitted (whose wavelength ranges in this analysis are listed in the first column of Table 1),  $\lambda_{ref}$  is a reference wavelength within the fitting region in question, adopted as the central wavelength automatically in AI-VPFIT. The parameters  $c_l$  and  $c_s$  are solved for simultaneously with the other absorption system model parameters. Further details are given in the VPFIT user guide Carswell & Webb (2023) and also in Webb et al. (2021a). Figure 1 illustrates the six different continuum models for each spectral segment in the combined dataset.

#### 5. 120 AI-VPFIT MODELS OF THE $Z_{ABS} = 1.7975$ SYSTEM TOWARDS PHL957

The extensive calculations reported here are based on AI-VPFIT (Lee et al. 2021a), which incorporates the VPFIT code, v12.4. Throughout the AI model construction

process, the Spectroscopic Information Criterion (SpIC) is used for model selection Webb et al. (2021b).

Many previous  $\Delta\alpha/\alpha$  measurements in the literature have not applied step (ii) above, i.e. the assumption has often been made that the original continuum is good so that no additional corrections were necessary, an assumption we show to be incorrect in this paper. Many published  $\Delta\alpha/\alpha$  measurements thus have quoted final error budgets that are too small; high precision  $\Delta\alpha/\alpha$  spectroscopic measurements should *always* account for this source of uncertainty.

#### 5.1. Modelling wavelength distortion

The focus of the present paper concerns the impact of continuum placement uncertainty on  $\Delta\alpha/\alpha$ . However, previous detailed studies of VLT/UVES and Keck/HIRES spectra have revealed an approximately linear wavelength distortion effect. This effect should not be ignored here since we aim to derive a realistic overall  $\Delta\alpha/\alpha$  uncertainty.

An explicit search for possible wavelength distortions in high-resolution quasar spectra was first reported in Molaro et al. (2008), who correlated the reflected solar spectrum (obtained from asteroid spectra observed using UVES on the VLT) with independent solar calibrations. The result of that initial study found no evidence for long-range wavelength distortion for VLT/UVES spectra. However, using higher precision data, Rahmani et al. (2013) showed that in fact long-range wavelength distortions can arise in UVES spectra, and that, *for constant observational instrument settings*, the distortion pattern can be approximated using a simple linear relationship between velocity shift and observed wavelength. However, a single linear distortion correction does not generally apply to quasar absorption system  $\Delta\alpha/\alpha$  measurements (as was done in Whitmore & Murphy (2015)) because, in many cases, final spectra are formed by co-adding multiple exposures with different observational settings. Instead, one must derive an appropriately weighted combination of shifted linear distortion patterns, taking into account instrument settings for all contributing exposures Dumont & Webb (2017). Additional free parameters for modelling potential distortion have been incorporated into AI-VPFIT and VPFIT version 12.4 Carswell & Webb (2023). This problem is also discussed in Appendix B of Webb et al. (2021a).

The distortion slopes measured for PHL957 in our AI-VPFIT calculations are given in Table 2, which show no significant evidence for long-range wavelength distortion. The first search for the presence of long-range wavelength distortion in the PHL957 spectrum used in the present paper was carried out as part of the PhD thesis research by Dumont (2018). In that study, the analysis was simpler; the two  $z_{abs} = 1.7975$  absorption system models given in King et al. (2012) were assumed, one based on thermal line broadening, the other based on turbulent broadening, and distortion parameters were solved for external to VPFIT. The Dumont & Webb (2017) approach is therefore slightly different to the AI-VPFIT analyses described in this paper, because here we use more realistic compound line broadening and solve for velocity structure and distortion parameters simultaneously. Nevertheless, interestingly, the slope parameters given

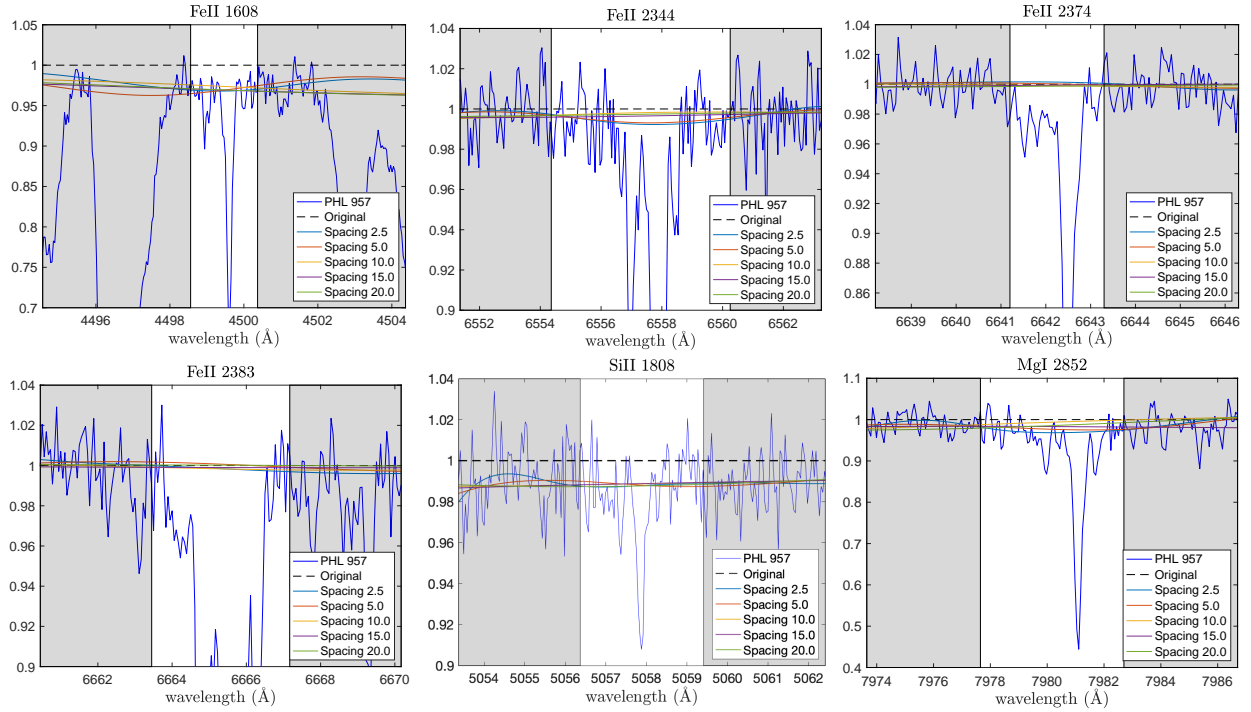


**Figure 1.** : PHL957  $z_{abs} = 1.7975$ : continua (prior to refinement) for each of the six spectral fitting regions (5 new, with different knot spacings, and the original continuum derived during the data reduction procedures).

	Knot spacing (Å)					
	2.5	5.0	10.0	15.0	20.0	Orig.
<b>Si II 1526</b>	0.004(1.3 $\sigma$ )	0.004(1.3 $\sigma$ )	0.004(1.2 $\sigma$ )	0.004(1.1 $\sigma$ )	0.005(1.4 $\sigma$ )	-0.007(-2.1 $\sigma$ )
4498.56-4500.37	6.366(0.4 $\sigma$ )	14.11(1.0 $\sigma$ )	7.710(0.5 $\sigma$ )	6.696(0.4 $\sigma$ )	7.489(0.5 $\sigma$ )	6.421(0.4 $\sigma$ )
<b>Fe II 1608</b>	0.007(3.2 $\sigma$ )	0.006 ( 2.9 $\sigma$ )	0.002(1.0 $\sigma$ )	0.007(3.1 $\sigma$ )	0.007(3.0 $\sigma$ )	-0.012(-2.5 $\sigma$ )
5056.37-5059.41	3.890(0.2 $\sigma$ )	-18.67(-1.0 $\sigma$ )	16.38(0.9 $\sigma$ )	13.10(0.7 $\sigma$ )	13.83(0.8 $\sigma$ )	-7.230(-0.2 $\sigma$ )
<b>Fe II 2344</b>	0.001(0.4 $\sigma$ )	0.000(0.0 $\sigma$ )	-0.003(-2.1 $\sigma$ )	-0.002(-1.1 $\sigma$ )	-0.002(-1.3 $\sigma$ )	-0.004(-2.0 $\sigma$ )
6554.36-6560.25	3.081(0.5 $\sigma$ )	2.196(0.4 $\sigma$ )	-0.427(-0.1 $\sigma$ )	-0.468(-0.1 $\sigma$ )	-1.551(-0.2 $\sigma$ )	-2.313(-0.4 $\sigma$ )
<b>Fe II 2374</b>	-0.010(-3.9 $\sigma$ )	-0.008(-3.5 $\sigma$ )	-0.007(-3.1 $\sigma$ )	-0.008(-3.2 $\sigma$ )	-0.007(-2.7 $\sigma$ )	-0.008(-3.3 $\sigma$ )
6641.20-6643.30	33.11(1.3 $\sigma$ )	34.28(1.3 $\sigma$ )	31.41(1.2 $\sigma$ )	27.04(1.1 $\sigma$ )	27.22(1.1 $\sigma$ )	28.91(1.2 $\sigma$ )
<b>Fe II 2383</b>	-0.006(-1.6 $\sigma$ )	-0.008(-2.5 $\sigma$ )	-0.006(-1.8 $\sigma$ )	-0.007(-2.1 $\sigma$ )	-0.007(-1.6 $\sigma$ )	-0.005(-1.0 $\sigma$ )
6663.45-6667.17	8.802(0.5 $\sigma$ )	10.42(0.7 $\sigma$ )	7.766(0.5 $\sigma$ )	6.885(0.5 $\sigma$ )	1.985(0.1 $\sigma$ )	-7.139(-0.3 $\sigma$ )
<b>Mg I 2851</b>	0.007(1.3 $\sigma$ )	0.001(0.2 $\sigma$ )	-0.013(-2.8 $\sigma$ )	-0.003(-0.5 $\sigma$ )	-0.004(-0.6 $\sigma$ )	-0.011(-0.9 $\sigma$ )
7977.65-7982.70	-3.707(-0.2 $\sigma$ )	7.379(0.4 $\sigma$ )	-21.39(-1.1 $\sigma$ )	-1.932(-0.1 $\sigma$ )	-30.55(-1.1 $\sigma$ )	-38.21(-0.9 $\sigma$ )

**Table 1:** AI-VPFIT continuum refinement parameters for each spectral segment used to fit  $\Delta\alpha/\alpha$  in the PHL957  $z_{abs} = 1.7975$  absorption system, for each initial continuum model. The leftmost column shows the six atomic species used, their rest-frame wavelengths, and underneath, the observed-frame fitting ranges in Å. The header shows knot spacings in Å. The rightmost column, “Orig.,” uses the continuum provided with the extracted spectrum (see Section 3). Each box shows  $\langle(c_l - 1)\rangle$  (upper row) and  $\langle c_s \rangle$  (lower). The quantities in brackets illustrate the statistical significance (and signs of) the deviations from  $c_l = 1$  and  $c_s = 0$ , i.e.  $\langle(c_l - 1)/\sigma(c_l)\rangle$  and  $\langle c_s/\sigma(c_s)\rangle$ .



in Dumont & Webb (2017) for the  $z_{abs} = 1.7975$  absorption system towards PHL957 are  $\gamma = 0.09 \pm 0.07$  (thermal broadening),  $0.26 \pm 0.08$  (turbulent broadening), and  $0.26 \pm 0.07$  (method of moments)  $\text{ms}^{-1} \text{\AA}^{-1}$ , consistent with the set of mean AI-VPFIT results given in Table 2, which lie in the range  $0.14 \pm 10 < \gamma < 0.18 \pm 10 \text{ms}^{-1} \text{\AA}^{-1}$ . Since the distortion parameters are included in the AI-VPFIT covariance matrix, distortion uncertainty propagates correctly to the final  $\Delta\alpha/\alpha$  uncertainty.

### 5.2. Impact of continuum uncertainty on $\Delta\alpha/\alpha$ measurement with VPFIT continuum refinement

Table 1 gives the continuum refinement parameters and their associated  $1\sigma$  uncertainties, for all six spectral segments used. Each box in the table contains  $(c_l - 1)/\sigma(c_l)$  (upper row) and  $c_s/\sigma(c_s)$  (lower), i.e. the quantities provide deviations from no-correction as multiples of 1 standard deviation, and thus illustrate whether or not the non-linear least squares procedure deemed the parameter to be statistically necessary. The uncertainties  $\sigma(c_l)$  and  $\sigma(c_s)$  are obtained from VPFIT’s parameter covariance matrix. Table 1 shows that 8 out of 36 continuum corrections require corrections with a significance level of  $3\sigma$  or larger, associated with 2 of the 6 spectral fitting regions, suggesting that corrections this large might be commonplace. This is interesting because it illustrates that even if the original continuum appears good (visually), as is the case for PHL957, local adjustments (i.e. for each fitting region) are likely to be needed.

Table 1 also shows that AI-VPFIT required an increasing number of components as the knot spacing increases, the largest number being required when AI-VPFIT was supplied with the original continuum. This trend is unsurprising because as the knot spacing is increased, the spline model tends to the (coarser) original continuum. The variation in the number of components does not indicate a preference for any particular continuum, but it does provide independent evidence that there is a source of uncertainty associated with continuum modelling that must be taken into account in the overall  $\Delta\alpha/\alpha$  error budget. However, the results illustrated in Table 1 do not show whether these local continuum adjustments have any impact on the measured  $\Delta\alpha/\alpha$ . We thus next examine the corresponding changes in  $\Delta\alpha/\alpha$ , with and without these corrections.

The calculations comprise: 20 independent models for each of 6 continuum  $\Delta\alpha/\alpha$  measurements (2.5, 5.0, 10.0, 15, 20  $\text{\AA}$  knot spacings, plus the original continuum) i.e. we have computed a total of 120 AI-VPFIT models for the  $z_{abs} = 1.7975$  absorption system. Figure 2 illustrates one example model (smallest SpIC, continuum knot spacing 10 $\text{\AA}$ ). Figure 3 illustrates the 120 individual  $\Delta\alpha/\alpha$  measurements. For each model, continuum parameters were included, allowing the initial continuum model to refine. The plotted error bar illustrates the statistical (covariance matrix) error. Insets show  $\langle\Delta\alpha/\alpha\rangle$ , the mean over 20 measurements and its associated point to point scatter for each set of 20 measurements  $\langle\sigma_s\rangle$ . This additional  $\Delta\alpha/\alpha$  scatter is caused by two effects: first, as the last row of Table 1 shows, small continuum variations give rise to slightly different kinematic structures with different numbers of absorption components. Second, it is well known that non-linear least squares methods with

many free parameters generally suffer from convergence issues e.g. Webb & Lee (2024). We have not attempted to quantify the balance between these two effects. Table 3 summarises the results illustrated in Figure 3. The upper and lower limits are the  $1\sigma$  uncertainties about the illustrated measurement, formed from the quadrature addition of the symmetric statistical uncertainty and the asymmetric convergence scatter.

Table 4 gives the analogous results where *no* continuum refinement parameters were included. Comparing this table with Table 3 therefore provides a check on whether, for this particular quasar measurement at least, continuum refinement had any effect. In all 6 comparisons, we see that  $\Delta\alpha/\alpha$  does indeed change when continuum refinement is applied. The magnitude of the mean shift is  $1.2 \times 10^{-6}$ , approximately 1/5 of the statistical  $\Delta\alpha/\alpha$  error bar, which itself correctly allows for the presence of the continuum refinement parameters since the latter is derived from the model covariance matrix.

### 5.3. What causes the discrepant result obtained using the original continuum?

Visual inspection (black continuous line in Figure 1) suggests that the initial, “unrefined”, continuum, “Orig.” in Tables 3 and 4, is reasonable. However, some deviations between that original continuum and the 5 new (unrefined) models are noticeable, particularly across two transitions, FeII 2344 and SiII 1808 $\text{\AA}$ . Nevertheless, the AI-VPFIT results illustrated in Figure 3 and summarised in Table 3 show that, even after refinement (i.e. AI-VPFIT optimisation of the  $c_s$  and  $c_l$  parameters for each spectral region), the refined original continuum gives  $\langle\Delta\alpha/\alpha\rangle = 3.2^{+6.1}_{-6.4} \times 10^{-6}$ , whereas all other measurements (based on a new initial continuum model derived using the method described in Section 2) are around  $-0.5 \times 10^{-6}$ , with very little scatter. Even after refinement of all 6 continua, i.e. including the original, the discrepancy between the original continuum and refined continuum results corresponds to  $\sim 67\%$  of the best statistical (i.e. covariance matrix) uncertainty and is therefore important.

To investigate the source of the effects described in the preceding paragraph, we carried out an additional set of 120 AI-VPFIT calculations, with continuum refinement, in which the initial continua for 5 (out of 6) spectral segments were the original ones, whilst the continuum for one remaining spectral segment at a time was replaced with the locally refined continuum. This was done for one specific knot spacing only (5 $\text{\AA}$ , because calculation times are fairly long). The results from these 120 new models are given in Table 5, which show the strongest impact arises when the Fe II 1608 $\text{\AA}$  continuum is replaced, suggesting the difference between the original and refined continua plays an more important role in this wavelength region (see Fig.1). Interestingly, Si II 1808 $\text{\AA}$  also displays a similarly large offset but this appears not to impact substantially in this case.

## 6. CONCLUSIONS AND DISCUSSION

The calculations presented in this paper have shown the importance of careful continuum preparation, *and* that the continuum model needs to be refined further, simultaneous with absorption system model optimisation,

Knots (Å)	2.5	5.0	10.0	15.0	20.0	Orig.
1	0.213 ± 0.092	0.160 ± 0.088	0.160 ± 0.089	0.119 ± 0.107	0.154 ± 0.087	0.062 ± 0.106
2	0.111 ± 0.108	0.221 ± 0.091	0.112 ± 0.107	0.210 ± 0.089	0.126 ± 0.106	0.182 ± 0.107
3	0.085 ± 0.109	0.241 ± 0.089	0.262 ± 0.088	0.262 ± 0.130	0.100 ± 0.106	0.150 ± 0.126
4	0.249 ± 0.089	0.092 ± 0.104	0.084 ± 0.109	0.262 ± 0.125	0.235 ± 0.089	0.129 ± 0.099
5	0.181 ± 0.092	0.090 ± 0.109	0.081 ± 0.110	0.093 ± 0.108	0.085 ± 0.109	0.179 ± 0.086
6	0.092 ± 0.102	0.244 ± 0.089	0.183 ± 0.131	0.233 ± 0.088	0.251 ± 0.089	0.191 ± 0.126
7	0.238 ± 0.089	0.101 ± 0.108	0.109 ± 0.108	0.086 ± 0.105	0.068 ± 0.107	0.172 ± 0.090
8	0.176 ± 0.096	0.340 ± 0.112	0.083 ± 0.109	0.080 ± 0.106	0.303 ± 0.106	0.134 ± 0.102
9	0.249 ± 0.089	0.074 ± 0.106	0.214 ± 0.091	0.148 ± 0.086	0.232 ± 0.090	0.114 ± 0.102
10	0.168 ± 0.094	0.320 ± 0.104	0.215 ± 0.092	0.085 ± 0.111	0.096 ± 0.098	0.162 ± 0.084
11	0.079 ± 0.110	0.078 ± 0.110	0.107 ± 0.104	0.094 ± 0.110	0.068 ± 0.108	0.184 ± 0.090
12	0.089 ± 0.112	0.080 ± 0.110	0.073 ± 0.106	0.231 ± 0.090	0.257 ± 0.088	0.273 ± 0.128
13	0.175 ± 0.091	0.098 ± 0.102	0.135 ± 0.097	0.163 ± 0.090	0.193 ± 0.090	0.344 ± 0.106
14	0.253 ± 0.089	0.235 ± 0.090	0.257 ± 0.088	0.241 ± 0.089	0.247 ± 0.091	0.299 ± 0.110
15	0.216 ± 0.092	0.117 ± 0.111	0.098 ± 0.107	0.191 ± 0.092	0.087 ± 0.110	0.210 ± 0.089
16	0.216 ± 0.091	0.107 ± 0.097	0.110 ± 0.109	0.227 ± 0.122	0.085 ± 0.110	0.078 ± 0.106
17	0.210 ± 0.092	0.217 ± 0.088	0.201 ± 0.122	0.067 ± 0.110	0.119 ± 0.110	0.176 ± 0.095
18	0.231 ± 0.087	0.089 ± 0.105	0.062 ± 0.105	0.190 ± 0.090	0.086 ± 0.118	0.256 ± 0.156
19	0.120 ± 0.107	0.241 ± 0.089	0.158 ± 0.092	0.194 ± 0.090	0.196 ± 0.097	0.180 ± 0.093
20	0.054 ± 0.111	0.108 ± 0.106	0.073 ± 0.109	0.068 ± 0.107	0.075 ± 0.109	0.167 ± 0.095
Means	0.170 ± 0.097	0.163 ± 0.101	0.139 ± 0.104	0.162 ± 0.102	0.153 ± 0.101	0.182 ± 0.105

**Table 2:** Best fit distortion slopes for the  $z_{abs} = 1.7975$  absorption system towards PHL957, in  $\text{ms}^{-1} \text{Å}^{-1}$ , for all 120 AI-VPFIT absorption system models. See Section 5.1 for details.

Knots (Å)	2.5	5.0	10.0	15.0	20.0	Orig.
$\langle \Delta\alpha/\alpha \rangle$	$-0.57^{+5.5}_{-5.6}$	$-0.47^{+5.5}_{-5.5}$	$-0.53^{+5.4}_{-5.5}$	$-0.41^{+5.5}_{-5.5}$	$-0.67^{+5.5}_{-5.6}$	$3.2^{+6.1}_{-6.4}$
$\langle N \rangle$	$7.75 \pm 1.07$	$7.70 \pm 1.03$	$8.05 \pm 0.76$	$8.05 \pm 0.83$	$8.00 \pm 1.34$	$9.65 \pm 1.35$

**Table 3:** PHL957  $z_{abs} = 1.7975$  with continuum refinement: the impact of using different quasar continuum models on measurements of  $\Delta\alpha/\alpha$  (in units of  $10^{-6}$ ). Six different continua are used (5 knot spacings plus original continuum). The automated continuum fitting parameters are all described in Lee et al. (2024). Six transitions are modelled simultaneously: Fe II 1608, Fe II 2344, Fe II 2374, Fe II 2383, Si II 1808, and Mg I 2853 Å. The asymmetric  $\Delta\alpha/\alpha$  uncertainties are formed from the symmetric statistical uncertainty in quadrature addition with the smaller asymmetric non-uniqueness scatter. The lowest row shows the mean number of heavy element absorption components (with  $1\sigma$  error). Averages are taken over the 20 AI-VPFIT models for each knot setting in all cases (see Figure 3 insets). See Section 5.2 for further details.

Knots (Å)	2.5	5.0	10.0	15.0	20.0	Orig.
$\langle \Delta\alpha/\alpha \rangle$	$0.91^{+5.6}_{-6.3}$	$1.2^{+5.7}_{-5.8}$	$1.0^{+5.7}_{-5.7}$	$-0.77^{+5.7}_{-5.7}$	$-1.0^{+5.6}_{-5.6}$	$4.9^{+6.4}_{-6.6}$
$\langle N \rangle$	$8.00 \pm 0.79$	$8.75 \pm 0.79$	$9.20 \pm 0.70$	$7.55 \pm 0.51$	$7.35 \pm 0.49$	$11.25 \pm 1.21$

**Table 4:** PHL957  $z_{abs} = 1.7975$ , without continuum refinement: same as Table 3 but no free continuum model parameters were included in AI-VPFIT modelling i.e. only the initial continuum models were used.  $\Delta\alpha/\alpha$  is in units of  $10^{-6}$ . The mean number of components is formed from an average over 20 models in each case.

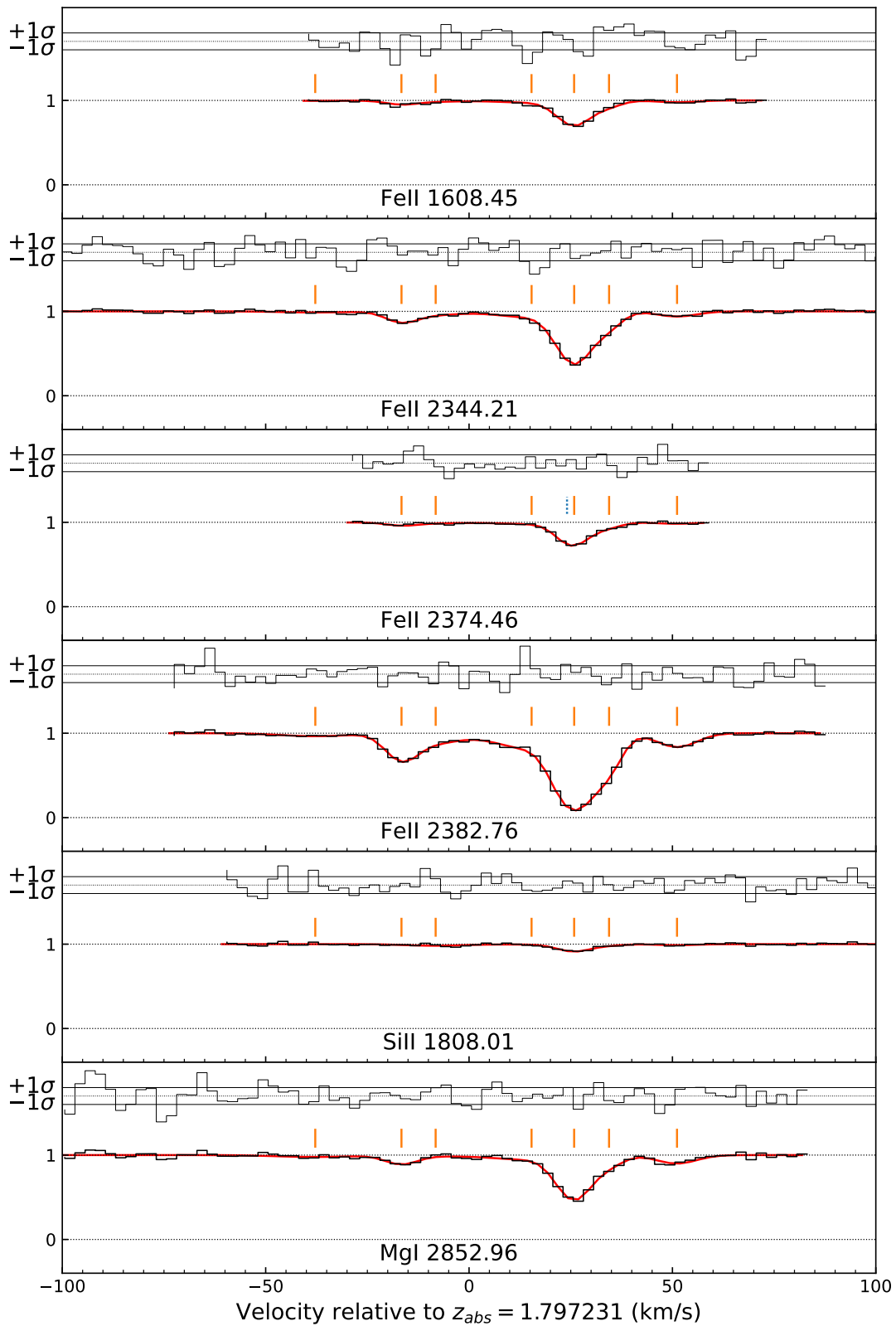
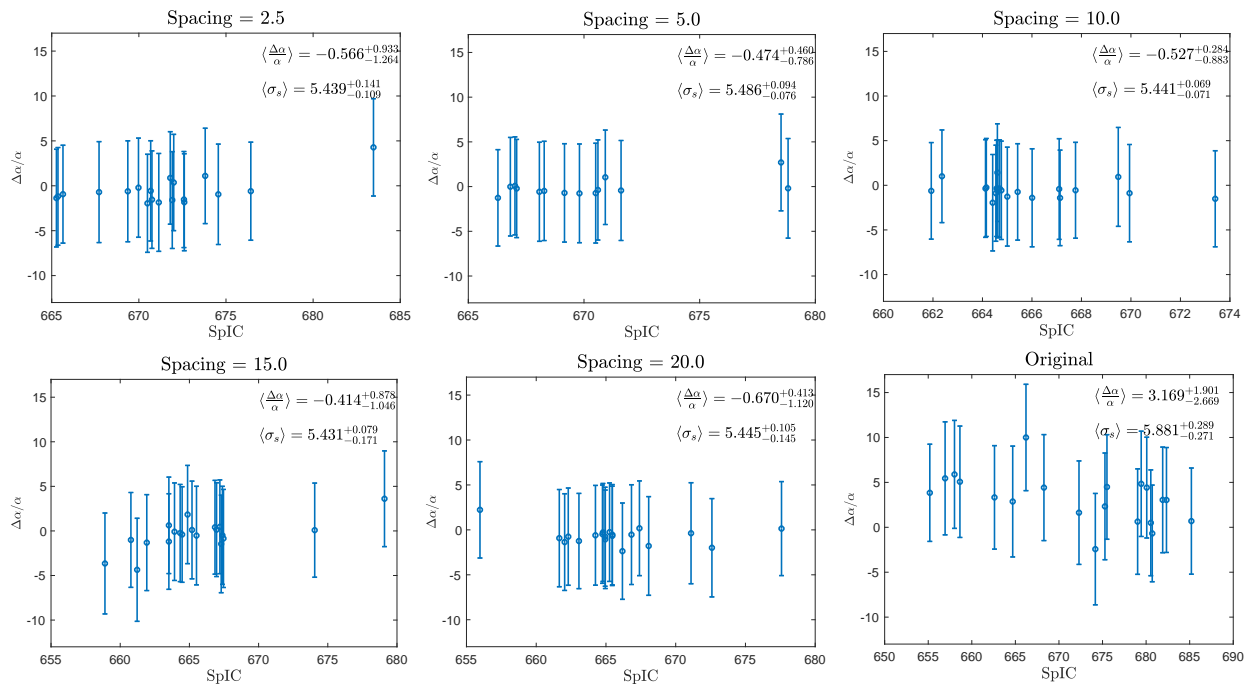


Figure 2. : Best AI-VPFIT/SpIC model with continuum knot spacing  $10\text{\AA}$



**Figure 3.** : 120  $\Delta\alpha/\alpha$  measurements from AI-VPFIT models of the  $z_{abs} = 1.7975$  absorption system towards PHL957 (20 independent AI-VPFIT  $\Delta\alpha/\alpha$  measurements for each of 6 continua). Free parameters to allow for any possible linear wavelength distortion were also included. See Section 5.2 for details.

<b>Replacement:</b>	Fe II 1608	Fe II 2344	Fe II 2374	Fe II 2383	Si II 1808	Mg I 2853
$\langle \Delta\alpha/\alpha \rangle$ :	$-0.49^{+5.5}_{-5.5}$	$1.9^{+6.0}_{-6.1}$	$2.8^{+6.4}_{-6.5}$	$3.5^{+6.3}_{-6.5}$	$3.0^{+6.2}_{-6.5}$	$2.6^{+6.0}_{-6.1}$

**Table 5:** PHL957  $z_{abs} = 1.7975$ : continuum replacement test carried out using the  $5\text{\AA}$  knot spacing continuum model. The asymmetric  $\Delta\alpha/\alpha$  uncertainties are formed from the symmetric statistical uncertainty in quadrature addition with the smaller asymmetric non-uniqueness scatter. Each  $\langle \Delta\alpha/\alpha \rangle$  value is the mean over 20 independently formed models.  $\Delta\alpha/\alpha$  is in units of  $10^{-6}$ . With no replacement, the refined original continuum gives  $\langle \Delta\alpha/\alpha \rangle = 3.2^{+6.1}_{-6.4} \times 10^{-6}$ . See Section 5.3 for details.

else a significant additional source of uncertainty may be added to a  $\Delta\alpha/\alpha$  measurement. This uncertainty has been ignored in many, even most, previous measurements. We have studied only a single absorption system, so do not know whether our results apply more broadly (although there is no reason to think they do not). The work presented in this paper should not be interpreted as a criticism of the original continua provided in the compilation of Murphy et al. (2019); that initial basic continuum is useful and provides an invaluable starting point for the more refined calculations described in this paper. With the caveat above, we draw the following conclusions, in the context of minimising systematic errors associated with  $\Delta\alpha/\alpha$  measurements:

1. Continuum uncertainty (as described by Eq. (4)) significantly alters  $\Delta\alpha/\alpha$  estimates. By “significantly”, we mean here that the additional uncertainty on  $\Delta\alpha/\alpha$  associated with continuum placement uncertainty is a non-negligible fraction of the statistical uncertainty on  $\Delta\alpha/\alpha$ . Thus, when attempting to continuum-fit high resolution quasar spectra, it is desirable to have an objective and reproducible method that avoids interactive human

decision making as far as possible.

2. In this study, we take a two-stage approach, (i) prior to any absorption system modelling, fit new continua, and then (ii) refine those continua simultaneous with absorption system modelling. In most previous searches for varying fundamental constants, this has not been done. Our findings suggest that if this is done, any systematic on the inferred  $\Delta\alpha/\alpha$  measurement may be reduced to a negligible level (i.e. far below the covariance matrix uncertainty) although further studies of other systems are needed to confirm this.
3. The 5 new models we derive (after fine-tuning, Table 3) produce consistent  $\Delta\alpha/\alpha$  results. We do not know if that consistency is generally true, but this one result clearly motivates checking for each new  $\Delta\alpha/\alpha$  measurement made and emphasises the necessity for a carefully derived continuum before attempting to model absorption profiles. Perhaps counter-intuitively, the  $\Delta\alpha/\alpha$  uncertainty estimate tends to decrease slightly, rather than increase, when additional continuum parameters are included in the modelling. The explanation



may in part be that an improved local continuum often (but not always) tends to reduce the number of absorption line components in the best-fit model.

4. In the case studied here, the original (unrefined) supplied continuum (despite appearing visually to be quite good) gives rise to a large systematic offset in the measured  $\Delta\alpha/\alpha$ , compared to the higher-order continuum models we calculated, with or without fine-tuning.
5. The  $z_{abs} = 1.7975$  absorption system towards PHL957 appears not to suffer from non-uniqueness problems Lee et al. (2021b), as Figure 3 shows. This absorption system therefore appears to be a “good” system for such measurements in that specific sense. Our example or illustrative result is  $\Delta\alpha/\alpha = -0.53_{-5.5}^{+5.4} \times 10^{-6}$ . However, during the course of the study reported in this paper, a parallel analysis was done to explore the impact of isotopic abundance assumptions on the inferred  $\Delta\alpha/\alpha$  measurement Webb et al. (2023). Magnesium is of particular concern in this respect because lines from its stable isotopes are more widely spaced in wavelength than most other species general used for  $\Delta\alpha/\alpha$  measurements (Berengut et al. 2005; Salumbides et al. 2006). This means that modelling line positions with profiles formed using relative isotopic abundances that are incorrect can produce artificial line shifts, emulating  $\Delta\alpha/\alpha \neq 0$  (Webb et al. 1999). The effect was subsequently investigated in several studies, e.g. Kozlov et al. (2004); Ashenfelter et al. (2004); Fenner et al. (2005); Agafonova et al. (2011); Webb et al. (2014). By considering 2 cases, terrestrial Mg isotopic abundances, and the extreme of 100%  $^{24}\text{Mg}$ , the study in Webb et al. (2023) quantified (by comparing two absorption systems in close redshift proximity) the systematic effect on  $\Delta\alpha/\alpha$ . The results obtained indicate that *unless* one can be quite sure of the actual relative Mg isotopic abundances (which will generally *not* be the case), it may be prudent to avoid using Mg altogether for varying  $\alpha$  measurements. Nevertheless, as Figure 2 illustrates, the MgI 2852.96Å transition was included in the AI-VPFIT models (the Mg isotopes used here were assumed to be terrestrial abundances). Whilst the  $\Delta\alpha/\alpha$  values reported in this study may therefore be biased by the inclusion of Mg, the relative changes between  $\Delta\alpha/\alpha$  values with and without continuum fine tuning (the main point of this paper) are valid.

In addition to searching for new physics via spacetime variations of fundamental constants, another important ELT science driver is the direct measurement of cosmological redshift drift using spectral features in quasar spectra, Sandage (1962) and e.g. Liske et al. (2008). At higher redshifts, where relatively few continuum segments remain devoid of absorption in the Lyman forest, it is notoriously hard to estimate the local continuum level. For redshift drift measurements, the line position precision required for the measurement of Lyman- $\alpha$

absorption line positions is 2 orders of magnitude greater than for  $\Delta\alpha/\alpha$  measurements, and it is possible that the impact of variations in the local continuum estimate may dominate other sources of uncertainty. The results presented in this paper motivate a careful investigation of that problem.

#### ACKNOWLEDGEMENTS

We are grateful for access to the OzSTAR supercomputer at the Centre for Astrophysics and Supercomputing at Swinburne University of Technology.

#### DATA AVAILABILITY

The astronomical data used in this study is publicly available from the ESO Archive. The continuum fitting code and AI-VPFIT result files are available from the authors on request. VPFIT is publicly available. AI-VPFIT will be released for general use at a later date (when a user guide has been completed).

#### REFERENCES

- Agafonova, I. I., Molaro, P., Levshakov, S. A., & Hou, J. L. 2011, *Astron. Astrophys.*, 529, A28, doi: [10.1051/0004-6361/201016194](https://doi.org/10.1051/0004-6361/201016194)
- Ashenfelter, T., Mathews, G. J., & Olive, K. A. 2004, *Phys. Rev. Lett.*, 92, 041102, doi: [10.1103/PhysRevLett.92.041102](https://doi.org/10.1103/PhysRevLett.92.041102)
- Berengut, J. C., Flambaum, V. V., & Kozlov, M. G. 2005, *Phys. Rev. A*, 72, 044501, doi: [10.1103/PhysRevA.72.044501](https://doi.org/10.1103/PhysRevA.72.044501)
- Carswell, R. F., & Webb, J. K. 2014, VPFIT: Voigt profile fitting program, Astrophysics Source Code Library, <http://ascl.net/1408.015>
- . 2023, VPFIT, <https://www.ast.cam.ac.uk/people/Bob.Carswell>
- Coleman, G., Carswell, R. F., Strittmatter, P. A., et al. 1976, *Astrophys. J.*, 207, 1, doi: [10.1086/154460](https://doi.org/10.1086/154460)
- Dumont, V. 2018, PhD thesis, School of Physics, UNSW Sydney, (doi: <https://doi.org/10.26190/unsworks/20677>), <http://hdl.handle.net/1959.4/60353>
- Dumont, V., & Webb, J. K. 2017, *Mon. Not. Roy. Astron. Soc.*, 468, 1568, doi: [10.1093/mnras/stx381](https://doi.org/10.1093/mnras/stx381)
- Dzuba, V. A., Flambaum, V. V., & Webb, J. K. 1999, *Phys. Rev. Lett.*, 82, 888, doi: [10.1103/PhysRevLett.82.888](https://doi.org/10.1103/PhysRevLett.82.888)
- Fenner, Y., Murphy, M. T., & Gibson, B. K. 2005, *Mon. Not. Roy. Astron. Soc.*, 358, 468, doi: [10.1111/j.1365-2966.2005.08781.x](https://doi.org/10.1111/j.1365-2966.2005.08781.x)
- Haro, G., & Luyten, W. J. 1962, *Boletín de los Observatorios Tonantzintla y Tacubaya*, 3, 37
- King, J. A., Webb, J. K., Murphy, M. T., et al. 2012, *Mon. Not. Roy. Astron. Soc.*, 422, 3370, doi: [10.1111/j.1365-2966.2012.20852.x](https://doi.org/10.1111/j.1365-2966.2012.20852.x)
- Kozlov, M. G., Korol, V. A., Berengut, J. C., Dzuba, V. A., & Flambaum, V. V. 2004, *Phys. Rev. A*, 70, 062108, doi: [10.1103/PhysRevA.70.062108](https://doi.org/10.1103/PhysRevA.70.062108)
- Lee, C.-C., Webb, J. K., Carswell, R. F., et al. 2023, *Monthly Notices of the Royal Astronomical Society*, 521, 850, doi: [10.1093/mnras/stad600](https://doi.org/10.1093/mnras/stad600)
- Lee, C.-C., Webb, J. K., Carswell, R. F., & Milaković, D. 2021a, *Mon. Not. Roy. Astron. Soc.*, 504, 1787, doi: [10.1093/mnras/stab977](https://doi.org/10.1093/mnras/stab977)
- Lee, C.-C., Webb, J. K., Dougan, D., Dzuba, V. A., & Flambaum, V. V. 2024, TBD, x, x, doi: [x](https://doi.org/x)
- Lee, C.-C., Webb, J. K., Milaković, D., & Carswell, R. F. 2021b, *Mon. Not. Roy. Astron. Soc.*, 507, 27, doi: [10.1093/mnras/stab2005](https://doi.org/10.1093/mnras/stab2005)
- Liske, J., Grazian, A., Vanzella, E., et al. 2008, *Mon. Not. Roy. Astron. Soc.*, 386, 1192, doi: [10.1111/j.1365-2966.2008.13090.x](https://doi.org/10.1111/j.1365-2966.2008.13090.x)
- Lowrance, J. L., Morton, D. C., Zucchino, P., Oke, J. B., & Schmidt, M. 1972, *Astrophys. J.*, 171, 233, doi: [10.1086/151275](https://doi.org/10.1086/151275)

- Molaro, P., Levshakov, S. A., Monai, S., et al. 2008, *Astron. Astrophys.*, 481, 559, doi: [10.1051/0004-6361:20078864](https://doi.org/10.1051/0004-6361:20078864)
- Murphy, M. T., Kacprzak, G. G., Savorgnan, G. A. D., & Carswell, R. F. 2019, *Mon. Not. Roy. Astron. Soc.*, 482, 3458, doi: [10.1093/mnras/sty2834](https://doi.org/10.1093/mnras/sty2834)
- Rahmani, H., Wendt, M., Srianand, R., et al. 2013, *Mon. Not. Roy. Astron. Soc.*, 435, 861, doi: [10.1093/mnras/stt1356](https://doi.org/10.1093/mnras/stt1356)
- Salumbides, E. J., Hannemann, S., Eikema, K. S. E., & Ubachs, W. 2006, *Monthly Notices of the Royal Astronomical Society: Letters*, 373, L41, doi: [10.1111/j.1745-3933.2006.00239.x](https://doi.org/10.1111/j.1745-3933.2006.00239.x)
- Sandage, A. 1962, *Astrophysical Journal*, 136, 319, doi: [10.1086/147385](https://doi.org/10.1086/147385)
- Webb, J. K., Carswell, R. F., & Lee, C.-C. 2021a, *Mon. Not. Roy. Astron. Soc.*, 508, 3620, doi: [10.1093/mnras/stab2895](https://doi.org/10.1093/mnras/stab2895)
- Webb, J. K., Flambaum, V. V., Churchill, C. W., Drinkwater, M. J., & Barrow, J. D. 1999, *Phys. Rev. Lett.*, 82, 884, doi: [10.1103/PhysRevLett.82.884](https://doi.org/10.1103/PhysRevLett.82.884)
- Webb, J. K., King, J. A., Murphy, M. T., et al. 2011, *Phys. Rev. Lett.*, 107, 191101, doi: [10.1103/PhysRevLett.107.191101](https://doi.org/10.1103/PhysRevLett.107.191101)
- Webb, J. K., & Lee, C.-C. 2024, *Mon. Not. Roy. Astron. Soc.*, 528, 6550, doi: [10.1093/mnras/stae306](https://doi.org/10.1093/mnras/stae306)
- Webb, J. K., Lee, C.-C., Carswell, R. F., & Milaković, D. 2021b, *Mon. Not. Roy. Astron. Soc.*, 501, 2268, doi: [10.1093/mnras/staa3551](https://doi.org/10.1093/mnras/staa3551)
- Webb, J. K., Lee, C.-C., & Milaković, D. 2022, *Universe*, 8, 266, doi: [10.3390/universe8050266](https://doi.org/10.3390/universe8050266)
- Webb, J. K., Lee, C.-C., Milakovic, D., et al. 2023, arXiv e-prints, arXiv:2401.00888, doi: [10.48550/arXiv.2401.00888](https://doi.org/10.48550/arXiv.2401.00888)
- Webb, J. K., Wright, A., Koch, F. E., & Murphy, M. T. 2014, *Memorie della Società Astronomica Italiana*, 85, 57
- Whitmore, J. B., & Murphy, M. T. 2015, *Mon. Not. Roy. Astron. Soc.*, 447, 446, doi: [10.1093/mnras/stu2420](https://doi.org/10.1093/mnras/stu2420)
- Zafar, T., Popping, A., & Péroux, C. 2013, *Astron. Astrophys.*, 556, A140, doi: [10.1051/0004-6361/201321153](https://doi.org/10.1051/0004-6361/201321153)
-